

# Magnetic ordering and structural distortion in Ru doped BaFe<sub>2</sub>As<sub>2</sub> single crystals studied by Neutron and X-ray diffraction

M. G. Kim, D. K. Pratt, G. E. Rustan, W. Tian, J. L. Zarestky, A. Thaler, S. L. Bud'ko, P. C. Canfield, R. J. McQueeney, A. Kreyssig, and A. I. Goldman  
*Ames Laboratory, U.S. DOE and Department of Physics and Astronomy  
Iowa State University, Ames, IA 50011, USA  
(Dated: March 23, 2022)*

We present a systematic investigation of the antiferromagnetic ordering and structural distortion for the series of Ba(Fe<sub>1-x</sub>Ru<sub>x</sub>)<sub>2</sub>As<sub>2</sub> compounds ( $0 \leq x \leq 0.246$ ). Neutron and x-ray diffraction measurements demonstrate that, unlike for the electron-doped compounds, the structural and magnetic transitions remain coincident in temperature. Both the magnetic and structural transitions are gradually suppressed with increased Ru concentration and coexist with superconductivity. For samples that are superconducting, we find strong competition between superconductivity, the antiferromagnetic ordering, and the structural distortion.

PACS numbers: 74.70.Xa, 75.25.-j, 74.25.Dw

## I. INTRODUCTION

After the discovery of FeAs based superconductors,<sup>1,2</sup> extensive studies using neutron and x-ray scattering techniques have revealed strong and unusual interconnections between structure, magnetism, and superconductivity. In the undoped parent compounds of the  $A\text{EFe}_2\text{As}_2$  ( $A\text{E} = \text{Ba}, \text{Sr}, \text{Ca}$ ) family, the tetragonal-to-orthorhombic transition and the paramagnetic-to-antiferromagnetic transition occur at the same temperature, implying a strong coupling between structure and magnetism.<sup>3-6</sup> Upon hole-doping with K on the Ba site or electron-doping with transition metals (e.g. Co, Ni, Rh, Pt, Pd) on the Fe site, the structural transition temperature ( $T_S$ ) and the antiferromagnetic (AFM) transition temperature ( $T_N$ ) are suppressed to lower temperatures.<sup>2,7-18</sup> The structural and AFM transitions split with  $T_S > T_N$  in transition-metal doped BaFe<sub>2</sub>As<sub>2</sub>,<sup>10,11,13-18</sup> whereas the transitions remain coincident in K doped BaFe<sub>2</sub>As<sub>2</sub>.<sup>2,7,8</sup> When both the structural and magnetic transitions are suppressed to sufficiently low temperatures, independent of the coincidence of  $T_S$  and  $T_N$ , superconductivity emerges and coexists with antiferromagnetism for some doping levels.<sup>16-18</sup> Moreover, in Co-, Rh-, and Ni-doped BaFe<sub>2</sub>As<sub>2</sub>, several neutron measurements manifest a distinctive suppression of the magnetic order parameter in the superconducting regime, which clearly indicates competition between AFM and superconductivity.<sup>16-18</sup> Additionally, high-resolution x-ray diffraction measurements on Co- and Rh-doped BaFe<sub>2</sub>As<sub>2</sub> have revealed the suppression of orthorhombic distortion below  $T_c$  illustrating an unusual magnetoelastic coupling in the form of emergent nematic order in the iron arsenides.<sup>17,19-21</sup>

In stark contrast to the doping studies mentioned above, hole-doping through the substitution of Cr<sup>22-24</sup> or Mn<sup>25-27</sup> on the Fe site results in very different behavior. Neither Ba(Fe<sub>1-x</sub>Cr<sub>x</sub>)<sub>2</sub>As<sub>2</sub> nor Ba(Fe<sub>1-x</sub>Mn<sub>x</sub>)<sub>2</sub>As<sub>2</sub> are superconducting at ambient pressure for any  $x$  and the suppression of the AFM order with increasing  $x$  is more gradual than for the electron-doped series. Furthermore, for Ba(Fe<sub>1-x</sub>Cr<sub>x</sub>)<sub>2</sub>As<sub>2</sub> the structural and magnetic transitions remain locked together up to  $x \approx 0.30$  where the stripe-like AFM structure is re-

placed by G-type AFM order as found for BaMn<sub>2</sub>As<sub>2</sub><sup>28</sup> and proposed for BaCr<sub>2</sub>As<sub>2</sub>.<sup>29</sup> For Ba(Fe<sub>1-x</sub>Mn<sub>x</sub>)<sub>2</sub>As<sub>2</sub>, the structural and AFM transitions remain locked together until  $x \geq 0.102$ , where the orthorhombic distortion abruptly vanishes.<sup>27</sup> We have previously proposed that, in the absence of the orthorhombic distortion, the AFM structure may be described by a two-Q ordering.<sup>27</sup>

Whereas all of the studies above describe measurements performed on either electron-doped or hole-doped materials, it is also important to consider the response of these systems to isoelectronic doping. For example, superconductivity is observed with a maximum  $T_c \sim 30$  K by the isoelectronic doping of P at the As site in BaFe<sub>2</sub>As<sub>2</sub>.<sup>30</sup> Furthermore, Klintberg *et al.*<sup>31</sup> have discussed the equivalence of chemical and physical pressure in BaFe<sub>2</sub>(As<sub>1-x</sub>P<sub>x</sub>)<sub>2</sub> by showing that the temperature-pressure phase diagrams are similar, but shifted for different  $x$ . Nevertheless, the maximum superconducting transition temperatures are identical. It is believed that superconductivity in this compound originates from steric effects arising from the smaller ionic radius of P. Only small modifications of the Fermi surface were observed.<sup>32</sup> Superconductivity has also been reported in Sr(Fe<sub>1-x</sub>Ru<sub>x</sub>)<sub>2</sub>As<sub>2</sub> compounds with  $T_c$  up to 20 K, but at much higher doping levels than required for the electron-doped series (e.g. Co, Ni, Rh).<sup>33,34</sup> Ru substitution on the Fe site in Ba(Fe<sub>1-x</sub>Ru<sub>x</sub>)<sub>2</sub>As<sub>2</sub> was recently reported to exhibit properties similar to the electron-doped BaFe<sub>2</sub>As<sub>2</sub> series but, again, at higher doping compositions.<sup>35-38</sup> The structural and AFM transition temperatures are suppressed with increasing  $x$  and superconductivity occurs at  $x \approx 0.16$ .

Thaler *et al.*<sup>37</sup> have made an interesting comparison between the phase diagrams of Ru-doped BaFe<sub>2</sub>As<sub>2</sub> and the parent BaFe<sub>2</sub>As<sub>2</sub> compound under pressure. Although the unit cell volume increases with Ru doping, they found a striking similarity between the phase diagrams for Ru doping and physical pressure when scaled by the lattice parameter  $c/a$  ratio. Only a single feature corresponding to a magnetic, structural, or joint magnetic/structural transition has been observed in resistance and magnetization data for Ba(Fe<sub>1-x</sub>Ru<sub>x</sub>)<sub>2</sub>As<sub>2</sub> ( $x \leq 0.37$ ), similar to what has been found for the nonsuper-

conducting hole-doped series, but quite different from the behavior of electron doped  $\text{BaFe}_2\text{As}_2$ . Interestingly, we note that in the case of P doping on the As site, a splitting between the structural and magnetic transitions was noted in resistance measurements, that increases with P concentration.<sup>39</sup> It is, therefore, particularly important to clarify the microscopic nature of the magnetic and/or structural transitions for the case of isoelectronic doping on the Fe site in  $\text{Ba}(\text{Fe}_{1-x}\text{Ru}_x)_2\text{As}_2$ , as well as the interaction between magnetism, structure and superconductivity in this series.

Here we report on magnetic neutron diffraction and high-resolution x-ray diffraction measurements on the series of  $\text{Ba}(\text{Fe}_{1-x}\text{Ru}_x)_2\text{As}_2$  compounds ( $0 \leq x \leq 0.246$ ) which demonstrate that, unlike the electron-doped compounds, the structural and magnetic transitions remain coincident in temperature. Similar to the electron-doped samples, however, we find strong competition between superconductivity, the AFM ordering and the structural distortion. The transition temperatures, magnitudes of the ordered magnetic moment, and the magnitude of the orthorhombic distortions in  $\text{Ba}(\text{Fe}_{1-x}\text{Ru}_x)_2\text{As}_2$  are compared with previous reports on  $\text{Ba}(\text{Fe}_{1-x}\text{Co}_x)_2\text{As}_2$  and  $\text{Ba}(\text{Fe}_{1-x}\text{Mn}_x)_2\text{As}_2$ .<sup>19,27,40</sup>

## II. EXPERIMENT

Single crystals of  $\text{Ba}(\text{Fe}_{1-x}\text{Ru}_x)_2\text{As}_2$  were grown out of a FeAs self-flux using conventional high temperature solution growth technique described in Ref.37. The compositions were measured at between 10 and 20 positions on samples from each growth batch using wavelength dispersive spectroscopy (WDS). The combined statistical and systematic error on the Ru composition is not greater than 5% (e.g.  $0.126 \pm 0.003$ , see Ref.37). Magnetization and temperature-dependent AC electrical resistance data ( $f = 16$  Hz,  $I = 3$  mA) were collected in a Quantum Design Magnetic Properties Measurement System using a Linear Research LR700 resistance bridge for the latter. Electrical contact was made to the sample using Epotek H20E silver epoxy to attach Pt wires in a four-probe configuration.

Neutron diffraction measurements were performed on the HB1A diffractometer at the High Flux Isotope Reactor at Oak Ridge National Laboratory using samples with a typical mass of approximately 25 mg. The beam collimators before the monochromator-between the monochromator and sample-between the sample and analyzer-between the analyzer and detector were  $48^\circ$ - $40^\circ$ - $40^\circ$ - $136^\circ$ . HB1A operates at a fixed incident neutron energy of 14.7 meV, and two pyrolytic graphite filters were employed to effectively eliminate higher harmonics in the incident beam. The samples were aligned such that the  $(HLL)$  reciprocal lattice plane was coincident with the scattering plane of the spectrometer, and were mounted in a closed-cycle refrigerator. The temperature dependence of the scattering was studied at several nuclear Bragg peak positions and at  $\mathbf{Q}_{\text{AFM}} = (\frac{1}{2} \frac{1}{2} L=\text{odd})$  positions corresponding to the AFM order in the parent and electron-doped  $\text{BaFe}_2\text{As}_2$  compounds.

The high-resolution, single-crystal x-ray diffraction measurements were performed on a four-circle diffractometer us-

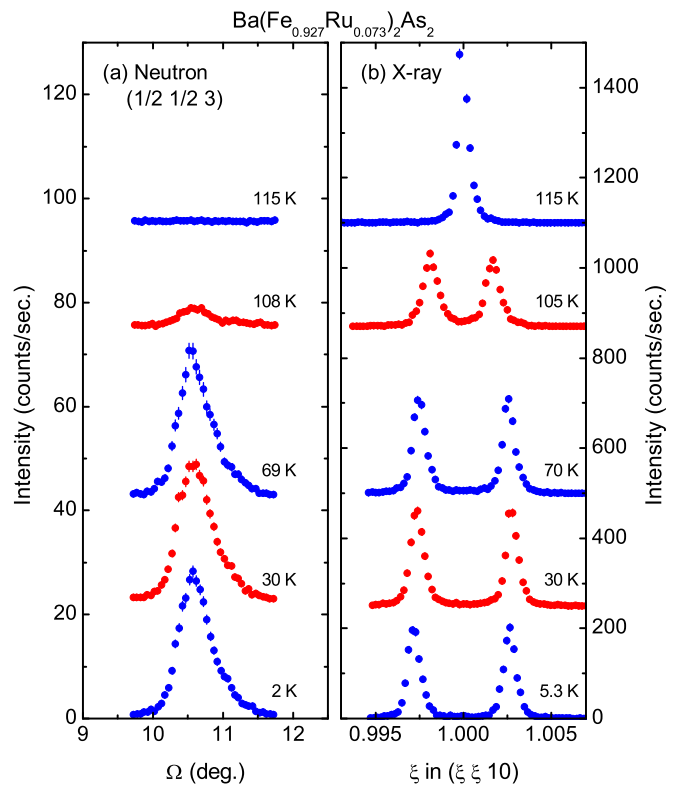


FIG. 1: (Color online) Temperature evolution of (a) the neutron diffraction rocking scans through the  $(\frac{1}{2} \frac{1}{2} 3)$  magnetic Bragg peak and (b) high-resolution x-ray diffraction  $[\xi\xi 0]$ -scans through the  $(1 1 10)$  Bragg peak in  $\text{Ba}(\text{Fe}_{0.927}\text{Ru}_{0.073})_2\text{As}_2$ . For this sample  $T_S = T_N = 109 \pm 1$  K. The data are shown with arbitrary offsets.

ing  $\text{Cu } K\alpha_1$  radiation from a rotating anode x-ray source, selected by a germanium (111) monochromator. For the temperature-dependence measurements, in addition to the parent  $\text{BaFe}_2\text{As}_2$ , we employed the same single crystals of  $\text{Ba}(\text{Fe}_{1-x}\text{Ru}_x)_2\text{As}_2$  ( $x = 0.073$  and  $0.205$ ) studied in our neutron measurements. The samples were attached to a flat copper sample holder on the cold finger of a closed-cycle duplex refrigerator. The sample mosaicities were less than  $0.02^\circ$  full-width-at-half-maximum (FWHM) as measured by rocking scans through the  $(1 1 10)$  reflection at room temperature. The diffraction data were obtained as a function of temperature between room temperature and 6 K, the base temperature of the refrigerator.

## III. RESULTS

Figures 1 (a) and (b) show neutron and x-ray data at selected temperatures for  $\text{Ba}(\text{Fe}_{1-x}\text{Ru}_x)_2\text{As}_2$  with  $x = 0.073$ . Above  $T_S = T_N = 109 \pm 1$  K, no scattering is observed at  $\mathbf{Q}_{\text{AFM}} = (\frac{1}{2} \frac{1}{2} 3)$ , but as the temperature is lowered below  $T_N$ , the scattering increases smoothly. The magnetic wave vector is identical to that for  $\text{BaFe}_2\text{As}_2$  compounds indicating that the magnetic structure is the same AFM stripe-like structure ob-

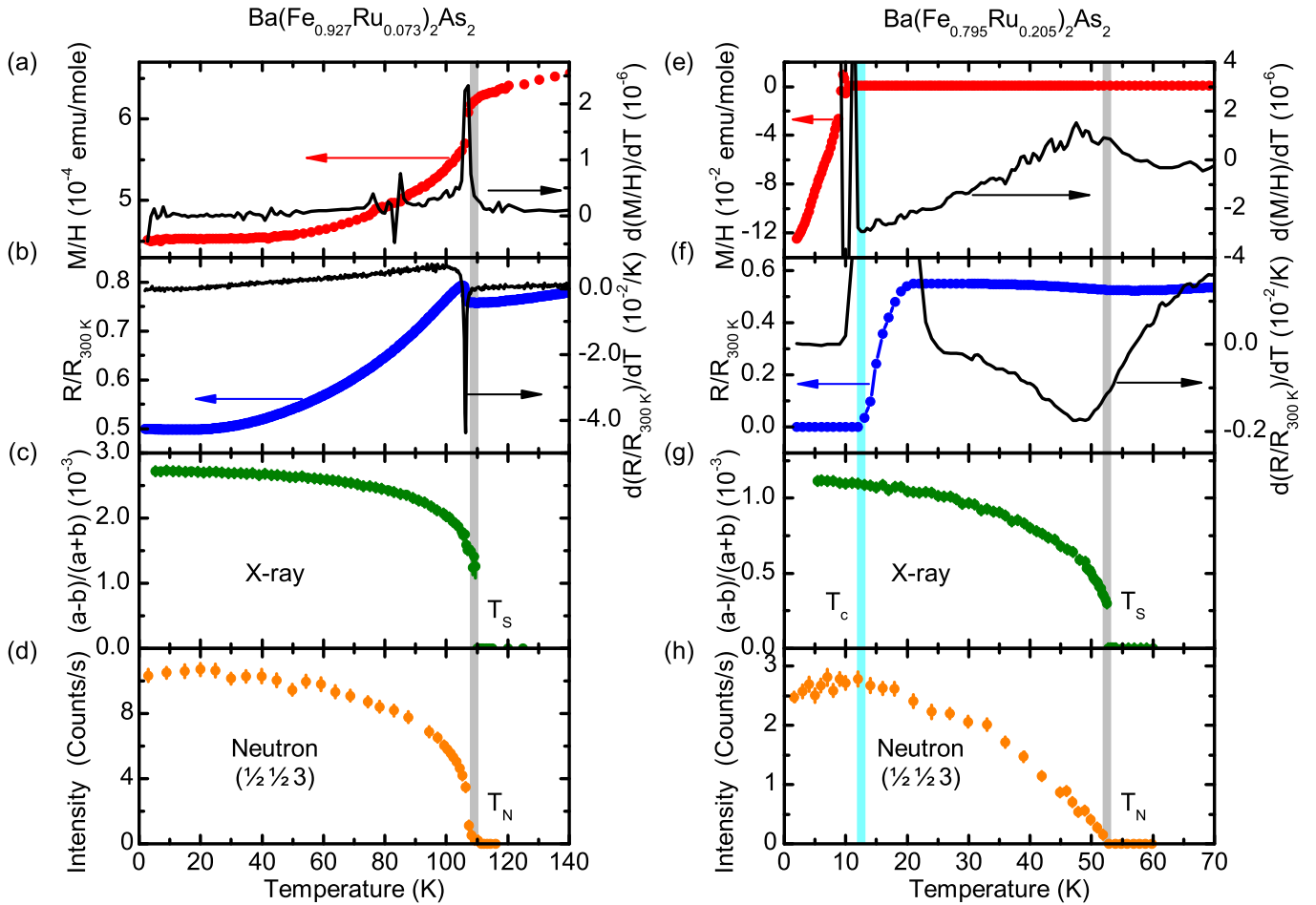


FIG. 2: (Color online) Plots of magnetization ( $\frac{M}{H}$ ) and its temperature derivative,  $\frac{d(\frac{M}{H})}{dT}$ , the resistance ratio ( $\frac{R}{R_{300\text{K}}}$ ) and its temperature derivative, the measured orthorhombic distortion ( $\delta = \frac{a-b}{a+b}$ ), and the integrated magnetic intensity at  $(\frac{1}{2} \frac{1}{2} 3)$  for  $\text{Ba}(\text{Fe}_{0.927}\text{Ru}_{0.073})_2\text{As}_2$  in panels (a)-(d) and  $\text{Ba}(\text{Fe}_{0.795}\text{Ru}_{0.205})_2\text{As}_2$  in panels (e)-(h). For  $x = 0.073$  the measured magnetization, resistance and their derivatives show sharp signatures at  $T_S = T_N = 107$  K, close to the value ( $109 \pm 1$  K) measured by the x-ray and neutron scattering measurements. For  $x = 0.205$ , the signatures at  $T_S = T_N$  are significantly broader. The maxima of the derivatives of the magnetization and resistance are found at 49 K whereas the x-ray and neutron scattering value is  $52 \pm 1$  K.

served for all AFM ordered  $A\text{EFe}_2\text{As}_2$  compounds ( $A\text{E} = \text{Ba}, \text{Sr}, \text{Ca}$ ), with AFM alignment of the moments along the orthorhombic **a** and **c** axes and FM alignment along the **b** axis. Analysis of the intensity ratios of different AFM reflections at selected temperatures confirmed that the moment direction is along the elongated orthorhombic **a** direction. From our high-resolution x-ray measurements we see [Fig. 1 (b)] that the  $(1\ 1\ 10)$  Bragg peak exhibits a sharp single peak above  $T_S = T_N = 109 \pm 1$  K consistent with a tetragonal structure and splits into two peaks below  $T_S$ , characteristic of the expected tetragonal-to-orthorhombic transition.

Figures 2 (a) and (b) summarize the magnetization and resistance measurements on  $\text{Ba}(\text{Fe}_{1-x}\text{Ru}_x)_2\text{As}_2$  with  $x = 0.073$ . A sharp feature attributed to  $T_S/T_N$  is observed at 107 K in the derivatives of magnetization and resistance. In Fig. 2 (c) and (d), the orthorhombic distortion,  $\delta = \frac{a-b}{a+b}$ , and the integrated magnetic scattering intensity, measured from rocking scans through  $Q_{\text{AFM}} = (\frac{1}{2} \frac{1}{2} 3)$ , are plotted as a func-

tion of temperature for  $x = 0.073$ . From these measurements we find that  $T_S = T_N = 109 \pm 1$  K, in reasonable agreement with the thermodynamic and transport measurements given the inherent uncertainty in assigning transition temperatures to features in the magnetization and resistance. Figures 2 (e) and (f) summarize the magnetization and resistance measurements on  $\text{Ba}(\text{Fe}_{1-x}\text{Ru}_x)_2\text{As}_2$  with  $x = 0.205$ . Here, we see that the characteristic features are much broader. According to the criteria of Ref.37,  $T_S/T_N$  is assigned to the maxima of the derivatives of magnetization and resistance, which is 49 K. The x-ray and neutron data of Figs. 2 (g) and (h) display the orthorhombic distortion  $\delta$  and the magnetic integrated intensity at  $Q_{\text{AFM}} = (\frac{1}{2} \frac{1}{2} 3)$  for  $x = 0.205$  and yield  $T_S = T_N = 52 \pm 1$  K. The transition temperatures derived from the criteria of Ref.37 are up to 3 K lower than the observed transition temperatures derived from the x-ray and neutron diffraction measurements. Most importantly, however, we find that, within experimental error, the structural and magnetic transitions re-

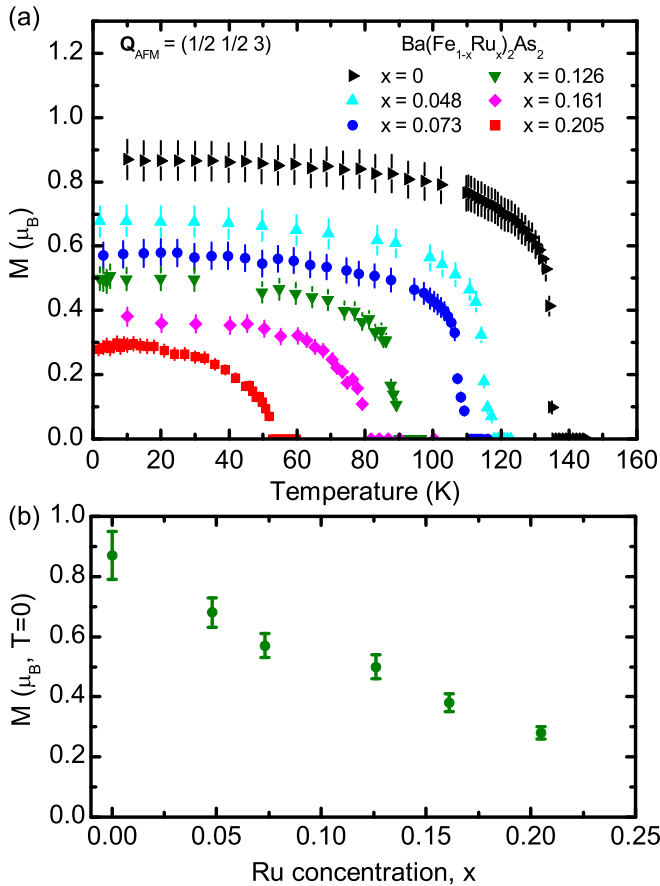


FIG. 3: (Color online) (a) Temperature dependence of the ordered magnetic moment calculated from the integrated intensity of the  $(\frac{1}{2}, \frac{1}{2}, 3)$  magnetic Bragg peak from  $\text{Ba}(\text{Fe}_{1-x}\text{Ru}_x)_2\text{As}_2$ . (b) The extrapolated ordered moment at zero temperature as a function of Ru concentration,  $x$ .

main locked together with increasing Ru doping and this behavior clearly differs from that found for the electron-doped compounds.

$\text{Ba}(\text{Fe}_{1-x}\text{Ru}_x)_2\text{As}_2$  crystals with  $x = 0, 0.048, 0.126,$  and  $0.161$  were also examined by neutron diffraction and the results for the entire series are summarized in Fig. 3. The magnetic integrated intensities were, again, determined from rocking scans through the magnetic peak at  $(\frac{1}{2}, \frac{1}{2}, 3)$  as a function of temperature and put on an absolute basis using the known mass of the samples and the magnetic diffraction from the parent compound,  $\text{BaFe}_2\text{As}_2$ , measured under identical conditions.<sup>40</sup> The ordered moment as a function of temperature for each sample is presented in Fig. 3(a), and the ordered moments extrapolated to  $T = 0$  are shown in Fig. 3(b). We see that as the Ru concentration increases, the ordered moment decreases monotonically.

Turning now to the effects of superconductivity on the AFM ordering and structural distortion, we first note that for the  $x = 0.205$  sample, the resistance and magnetization data show the existence of superconductivity below  $T_c \approx 13$  K in Figs. 2 (e) and (f). For this sample, in Fig. 2 (h), we observe a suppres-

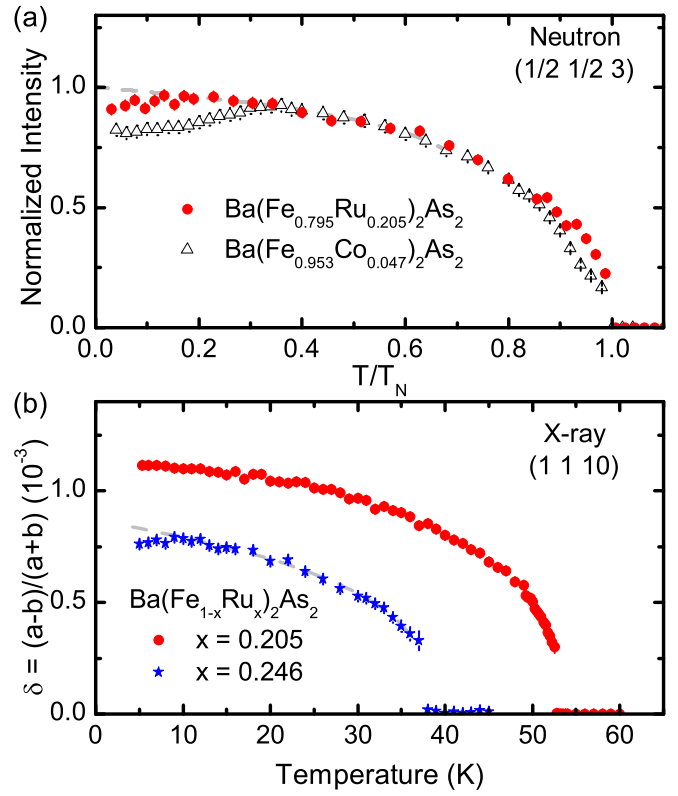


FIG. 4: (Color online)(a) Comparison of the suppression of AFM order below  $T_c$  between the 20.5% Ru (filled circles) and the 4.7% Co (open triangles)<sup>40</sup> doped  $\text{BaFe}_2\text{As}_2$  samples. Intensities are normalized for comparison. (b) Orthorhombic distortion for  $\text{Ba}(\text{Fe}_{1-x}\text{Ru}_x)_2\text{As}_2$  with  $x = 0.205$  (circles) and  $0.246$  (stars). The reduction in the distortion below  $T_c$  is not clearly observable for  $x = 0.205$  but it is evident for  $x = 0.246$ . The gray dashed lines are guides for eyes.

sion of the AFM order below  $T_c$  similar to what has been reported previously for Co-, Rh-, and Ni-doped  $\text{BaFe}_2\text{As}_2$ ,<sup>16-18</sup> where the presence of both AFM and superconductivity has been attributed to microscopically coexisting states that compete for the same itinerant electrons. It has also been established that the onset of superconductivity leads to a suppression of the orthorhombic distortion in the electron-doped compounds. Refs.19 and 17, for example, described this effect below  $T_c$  for both Co- and Rh-doped  $\text{BaFe}_2\text{As}_2$ , respectively. Because  $\frac{T_c}{T_N}$  for  $\text{Ba}(\text{Fe}_{0.795}\text{Ru}_{0.205})_2\text{As}_2$  is approximately half the value of  $\frac{T_c}{T_N}$  for  $\text{Ba}(\text{Fe}_{0.953}\text{Co}_{0.047})_2\text{As}_2$ , the magnitude of suppression of AFM order at the base temperature of our measurement is correspondingly smaller [Fig. 4 (a)], and the reduction of the orthorhombic distortion is not clearly observed [Figs. 2 (g) and 4(b)]. Therefore, we have also studied an additional concentration,  $x = 0.246 \pm 0.005$  ( $T_c \approx 14$  K), by high-resolution x-ray diffraction and, as shown in Fig. 4 (b), see the suppression of the orthorhombic distortion below  $T_c$ .

#### IV. DISCUSSION AND SUMMARY

Together with our previous investigations of  $\text{Ba}(\text{Fe}_{1-x}\text{Co}_x)_2\text{As}_2$  and  $\text{Ba}(\text{Fe}_{1-x}\text{Mn}_x)_2\text{As}_2$ , we now have a more complete picture of the effects of electron, hole and isoelectronic doping on the Fe site in the  $\text{BaFe}_2\text{As}_2$  compound. The compositional phase diagrams for all three doping series are shown in Fig. 5. Summarizing the trends illustrated in Fig. 5 (a) we see that for the Co-doped series, at low doping, the magnetic and structural transitions split with increasing Co concentration, superconductivity emerges over a finite compositional range and coexists with AFM order over an even more limited range of Co doping. The back-bending of the AFM and structural distortion phase lines in the superconducting region identify the reentrance of the paramagnetic and tetragonal phases at low temperature. Figs. 5 (a) and (b) display both the similarities and differences between  $\text{Ba}(\text{Fe}_{1-x}\text{Co}_x)_2\text{As}_2$  and  $\text{Ba}(\text{Fe}_{1-x}\text{Ru}_x)_2\text{As}_2$ . As found for Co substitution, Ru doping results in the suppression of the AFM and structural transitions and superconductivity emerges over a finite range of Ru concentration. The suppression of both the AFM order and orthorhombic distortion in the superconducting region suggests that reentrance of the paramagnetic tetragonal phase may also be found at some Ru doping concentration as well. However, for Ru doping the AFM and structural transitions remain locked together over an extended compositional range with respect to the phase diagram for Co doping. In Fig. 5 (c), we reproduce the compositional phase diagram for Mn doping, which is quite different from what is found for either Co or Ru substitution on the Fe site. Superconductivity is not in evidence at any Mn concentration and, while the AFM and structural transitions remain locked together with increasing Mn concentration, as found for  $\text{Ba}(\text{Fe}_{1-x}\text{Ru}_x)_2\text{As}_2$ , the structural distortion abruptly disappears for Mn doping in excess of  $x > 0.102$  although the AFM Bragg peak characteristic of stripe-like ordering persists. The latter observation is quite puzzling since all models for stripe-like ordering in the iron arsenides anticipate an attendant orthorhombic distortion due to magnetoelastic effects. However, we have previously proposed that the scattering at  $\mathbf{Q}_{\text{AFM}} = (\frac{1}{2}, \frac{1}{2}, L=\text{odd})$  positions may also be explained by the presence of a two- $\mathbf{Q}$  magnetic structure that is again consistent with tetragonal symmetry.<sup>27</sup>

It is clear that the interactions associated with structural, magnetic and superconducting instabilities in the  $\text{AEFe}_2\text{As}_2$  compounds are finely balanced and can be readily tuned through chemical substitution as well as pressure. For example, similarities between chemical doping and pressure were previously discussed for K doping on the Ba site.<sup>41</sup> For electron doping on the Fe site, a rigid band picture appears to be applicable, at least to first order, in explaining the phenomenology of magnetism, structure and superconductivity. Doping with Mn, however, clearly introduces strong perturbations on both the electronic and chemical structure, likely as a consequence of the more localized nature of the Mn magnetic moment. Doping with Ru provides a new interesting case study where, nominally, no electrons or holes are added to the system although the first band-structure calculations indicated

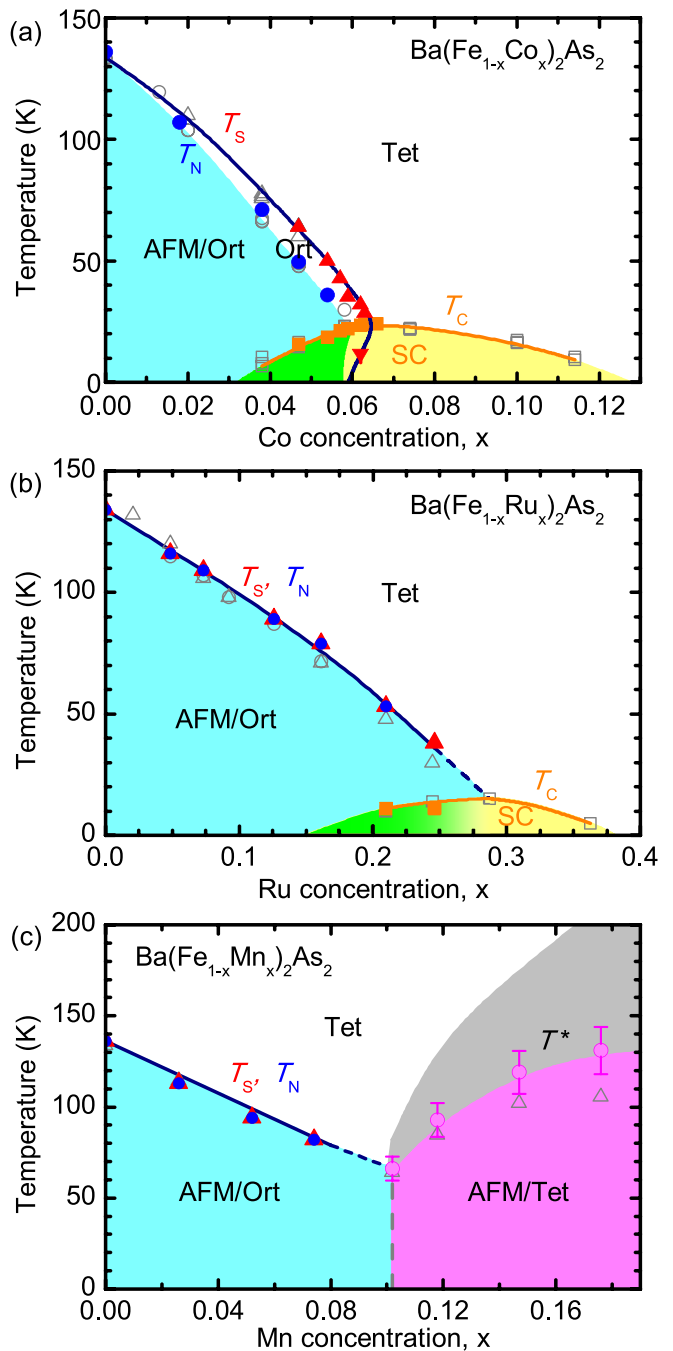


FIG. 5: (Color online) Compositional phase diagrams for (a)  $\text{Ba}(\text{Fe}_{1-x}\text{Co}_x)_2\text{As}_2$  from Ref.19, (b)  $\text{Ba}(\text{Fe}_{1-x}\text{Ru}_x)_2\text{As}_2$  from the present work and Ref.37, and (c)  $\text{Ba}(\text{Fe}_{1-x}\text{Mn}_x)_2\text{As}_2$  from Ref.27. The gray open triangles and open circles denote data taken from resistance and magnetization data respectively. The gray open squares denote bulk measurements of  $T_c$ . Filled red triangles denote  $T_S$  measured by x-ray diffraction, filled blue circles denote  $T_N$  measured by neutron diffraction, and the filled orange squares represent values for  $T_c$  from the x-ray and neutron data. Filled magenta circles denote  $T^*$  determined for the Mn doped sample by neutron measurements (see Ref.27).

that Ru substitution introduces additional electron carriers.<sup>35</sup> However, Hall effect and angle-resolved photoemission spectroscopy measurements,<sup>36,42</sup> have shown that the Ru substitution does not induce electron or hole doping, but does strongly modify the electronic structure by increasing both the number of carriers and their mobility by reducing correlation effects.

Summarizing, we have presented a systematic investigation of the AFM ordering and structural distortion on the series of  $\text{Ba}(\text{Fe}_{1-x}\text{Ru}_x)_2\text{As}_2$  compounds ( $0 \leq x \leq 0.246$ ). Our neutron and x-ray diffraction measurements demonstrate that, unlike the behavior found for the electron-doped compounds, the structural and magnetic transitions remain coincident in temperature, as also observed for low Mn doping. Both the magnetic and structural transitions are gradually suppressed with increased Ru concentration but, in contrast to the case for Mn doping where superconductivity is absent, AFM order

coexists with superconductivity. In the superconducting samples, we find a strong competition between superconductivity, the AFM ordering and the structural distortion.

We acknowledge valuable discussions with J. Schmalian and R. M. Fernandes. This work was supported by the Division of Materials Sciences and Engineering, Office of Basic Energy Sciences, U.S. Department of Energy. Ames Laboratory is operated for the U.S. Department of Energy by Iowa State University under Contract No. DE-AC02-07CH11358. The work at the High Flux Isotope Reactor, Oak Ridge National Laboratory (ORNL), was sponsored by the Scientific User Facilities Division, Office of Basic Energy Sciences, U.S. Department of Energy (U.S. DOE). ORNL is operated by UT-Battelle, LLC for the U.S. DOE under Contract No. DE-AC05-00OR22725.

- 
- <sup>1</sup> Y. Kamihara, T. Watanabe, M. Hirano, and H. Hosono, *J. Am. Chem. Soc.* **130**, 3296 (2008).
  - <sup>2</sup> M. Rotter, M. Tegel, and D. Johrendt, *Phys. Rev. Lett.* **101**, 107006 (2008).
  - <sup>3</sup> M. Rotter, M. Tegel, D. Johrendt, I. Schellenberg, W. Hermes, and R. Pöttgen, *Phys. Rev. B* **78**, 020503(R) (2008).
  - <sup>4</sup> Q. Huang, Y. Qiu, W. Bao, M. A. Green, J. W. Lynn, Y. C. Gasparovic, T. Wu, G. Wu, and X. H. Chen, *Phys. Rev. Lett.* **101**, 257003 (2008).
  - <sup>5</sup> A. Jesche, N. Caroca-Canales, H. Rosner, H. Borrmann, A. Ormeci, D. Kasinathan, H. H. Klauss, H. Luetkens, R. Khasanov, A. Amato, et al., *Phys. Rev. B* **78**, 180504(R) (2008).
  - <sup>6</sup> A. I. Goldman, D. N. Argyriou, B. Ouladdiaf, T. Chatterji, A. Kreyssig, S. Nandi, N. Ni, S. L. Bud'ko, P. C. Canfield, and R. J. McQueeney, *Phys. Rev. B* **78**, 100506(R) (2008).
  - <sup>7</sup> H. Chen, Y. Ren, Y. Qiu, W. Bao, R. H. Liu, G. Wu, T. Wu, Y. L. Xie, X. F. Wang, Q. Huang, et al., *Europhys. Lett.* **85**, 17006 (2009).
  - <sup>8</sup> D. S. Inosov, A. Leineweber, X. Yang, J. T. Park, N. B. Christensen, R. Dinnebier, G. L. Sun, C. Niedermayer, D. Haug, P. W. Stephens, et al., *Phys. Rev. B* **79**, 224503 (2009).
  - <sup>9</sup> S. R. Saha, T. Drye, K. Kirshenbaum, N. P. Butch, P. Y. Zavalij, and J. Paglione, *J. Phys.: Condens. Matter* **22**, 072204 (2010).
  - <sup>10</sup> A. S. Sefat, R. Jin, M. A. McGuire, B. C. Sales, D. J. Singh, and D. Mandrus, *Phys. Rev. Lett.* **101**, 117004 (2008).
  - <sup>11</sup> N. Ni, M. E. Tillman, J.-Q. Yan, A. Kracher, S. T. Hannahs, S. L. Bud'ko, and P. C. Canfield, *Phys. Rev. B* **78**, 214515 (2008).
  - <sup>12</sup> C. Lester, J.-H. Chu, J. G. Analytis, S. C. Capelli, A. S. Erickson, C. L. Condon, M. F. Toney, I. R. Fisher, and S. M. Hayden, *Phys. Rev. B* **79**, 144523 (2009).
  - <sup>13</sup> L. J. Li, Y. K. Luo, Q. B. Wang, H. Chen, Z. Ren, Q. Tao, Y. K. Li, X. Lin, M. He, Z. W. Zhu, et al., *New J. Phys.* **11**, 025008 (2009).
  - <sup>14</sup> N. Ni, A. Thaler, A. Kracher, J. Q. Yan, S. L. Bud'ko, and P. C. Canfield, *Phys. Rev. B* **80**, 024511 (2009).
  - <sup>15</sup> L. W. Harriger, A. Schneidewind, S. Li, J. Zhao, Z. Li, W. Lu, X. Dong, F. Zhou, Z. Zhao, J. Hu, et al., *Phys. Rev. Lett.* **103**, 087005 (2009).
  - <sup>16</sup> D. K. Pratt, W. Tian, A. Kreyssig, J. L. Zarestky, S. Nandi, N. Ni, S. L. Bud'ko, P. C. Canfield, A. I. Goldman, and R. J. McQueeney, *Phys. Rev. Lett.* **103**, 087001 (2009).
  - <sup>17</sup> A. Kreyssig, M. G. Kim, S. Nandi, D. K. Pratt, W. Tian, J. L. Zarestky, N. Ni, A. Thaler, S. L. Bud'ko, P. C. Canfield, et al., *Phys. Rev. B* **81**, 134512 (2010).
  - <sup>18</sup> M. Wang, H. Luo, J. Zhao, C. Zhang, M. Wang, K. Marty, S. Chi, J. W. Lynn, A. Schneidewind, S. Li, et al., *Phys. Rev. B* **81**, 174524 (2010).
  - <sup>19</sup> S. Nandi, M. G. Kim, A. Kreyssig, R. M. Fernandes, D. K. Pratt, A. Thaler, N. Ni, S. L. Bud'ko, P. C. Canfield, J. Schmalian, et al., *Phys. Rev. Lett.* **104**, 057006 (2010).
  - <sup>20</sup> C. Fang, H. Yao, W.-F. Tsai, J. P. Hu, and S. A. Kivelson, *Phys. Rev. B* **77**, 224509 (2008).
  - <sup>21</sup> C. Xu, M. Müller, and S. Sachdev, *Phys. Rev. B* **78**, 020501(R) (2008).
  - <sup>22</sup> A. S. Sefat, D. J. Singh, L. H. VanBebber, Y. Mozharivskiy, M. A. McGuire, R. Jin, B. C. Sales, V. Keppens, and D. Mandrus, *Phys. Rev. B* **79**, 224524 (2009).
  - <sup>23</sup> S. L. Bud'ko, S. Nandi, N. Ni, A. Thaler, A. Kreyssig, A. Kracher, J.-Q. Yan, A. I. Goldman, and P. C. Canfield, *Phys. Rev. B* **80**, 014522 (2009).
  - <sup>24</sup> K. Marty, A. D. Christianson, C. H. Wang, M. Matsuda, H. Cao, L. H. VanBebber, J. L. Zarestky, D. J. Singh, A. S. Sefat, and M. D. Lumsden, arXiv:1009.1818 (2010), unpublished.
  - <sup>25</sup> J. S. Kim, S. Khim, H. J. Kim, M. J. Eom, J. M. Law, R. K. Kremer, J. H. Shim, and K. H. Kim, *Phys. Rev. B* **82**, 024510 (2010).
  - <sup>26</sup> Y. Liu, D. L. Sun, J. T. Park, and C. T. Lin, *Physica C* (2010), in press.
  - <sup>27</sup> M. G. Kim, A. Kreyssig, A. Thaler, D. K. Pratt, W. Tian, J. L. Zarestky, M. A. Green, S. L. Bud'ko, P. C. Canfield, R. J. McQueeney, et al., *Phys. Rev. B* (2010), in press, arXiv:1011.2816.
  - <sup>28</sup> Y. Singh, M. A. Green, Q. Huang, A. Kreyssig, R. J. McQueeney, D. C. Johnston, and A. I. Goldman, *Phys. Rev. B* **80**, 100403(R) (2009).
  - <sup>29</sup> D. J. Singh, A. S. Sefat, M. A. McGuire, B. C. Sales, D. Mandrus, L. H. VanBebber, and V. Keppens, *Phys. Rev. B* **79**, 094429 (2009).
  - <sup>30</sup> S. Jiang, H. Xing, G. Xuan, C. Wang, Z. Ren, C. Feng, J. Dai, Z. Xu, and G. Cao, *J. Phys.: Condens. Matter* **21**, 382203 (2009).
  - <sup>31</sup> L. E. Klintberg, S. K. Goh, S. Kasahar, Y. Nakai, K. Ishida, M. Sutherland, T. Shibauchi, Y. Matsuda, and T. Terashima, *J. Phys. Soc. Jpn.* **79**, 123706 (2010).
  - <sup>32</sup> H. Shishido, A. F. Bangura, A. I. Coldea, S. Tonegawa, K. Hashimoto, S. Kasahara, P. M. C. Rourke, H. Ikeda,

- T. Terashima, R. Settai, et al., *Phys. Rev. Lett.* **104**, 057008 (2010).
- <sup>33</sup> W. Schnelle, A. Leithe-Jasper, R. Gumeniuk, U. Burkhardt, D. Kasinathan, and H. Rosner, *Phys. Rev. B* **79**, 214516 (2009).
- <sup>34</sup> Y. Qi, L. Wang, Z. Gao, W. Wang, X. Zhang, and Y. Ma, *Physica C* **469**, 1921 (2009).
- <sup>35</sup> S. Sharma, A. Bharathi, S. Chandra, V. R. Reddy, S. Paulraj, A. T. Satya, V. S. Sastry, A. Gupta, and C. S. Sundar, *Phys. Rev. B* **81**, 174512 (2010).
- <sup>36</sup> F. Rullier-Albenque, D. Colson, A. Forget, P. Thuéry, and S. Poissonnet, *Phys. Rev. B* **81**, 224503 (2010).
- <sup>37</sup> A. Thaler, N. Ni, A. Kracher, J. Q. Yan, S. L. Bud'ko, and P. C. Canfield, *Phys. Rev. B* **82**, 014534 (2010).
- <sup>38</sup> H. Hodovanets, E. D. Mun, A. Thaler, S. L. Bud'ko, and P. C. Canfield, arXiv:1010.5111 (2010), unpublished.
- <sup>39</sup> S. Kasahara, T. Shibauchi, K. Hashimoto, K. Ikada, S. Tonegawa, R. Okazaki, H. Shishido, H. Ikeda, H. Takeya, K. Hirata, et al., *Phys. Rev. B* **81**, 184519 (2010).
- <sup>40</sup> R. M. Fernandes, D. K. Pratt, W. Tian, J. Zarestky, A. Kreyssig, S. Nandi, M. G. Kim, A. Thaler, N. Ni, P. C. Canfield, et al., *Phys. Rev. B* **81**, 140501(R) (2010).
- <sup>41</sup> S. A. J. Kimber, A. Kreyssig, Y.-Z. Zhang, H. O. Jeschke, R. Valenti, F. Yokaichiya, E. Colombier, J. Yan, T. C. Hansen, T. Chatterji, et al., *Nat. Mater.* **8**, 471 (2009).
- <sup>42</sup> V. Brouet, F. Rullier-Albenque, M. Marsi, B. Mansart, M. Aichhorn, S. Biermann, J. Faure, L. Perfetti, A. Taleb-Ibrahimi, P. Le Fèvre, et al., *Phys. Rev. Lett.* **105**, 087001 (2010).